ARCHIVES OF ELECTRICAL ENGINEERING VOL. 65(1), pp. 73-86 (2016)

DOI 10.1515/aee-2016-0006

# Operating point resolved loss computation in electrical machines

GEORG VON PFINGSTEN, ANDREAS RUF, SIMON STEENTJES, MARCO HOMBITZER, DAVID FRANCK, KAY HAMEYER

*RWTH Aachen University*
*Institute of Electrical Machines*
*Schinkelstrasse 4, Aachen 52062, Germany*
*e-mail: georg.vonpfingsten@iem.rwth-aachen.de*

(Received: 12.08.2015, revised: 22.09.2015)

**Abstract:** Magnetic circuits of electromagnetic energy converters, such as electrical machines, are nowadays highly utilized. This proposition is intrinsic for the magnetic as well as the electric circuit and depicts that significant enhancements of electrical machines are difficult to achieve in the absence of a detailed understanding of underlying effects. In order to improve the properties of electrical machines the accurate determination of the locally distributed iron losses based on idealized model assumptions solely is not sufficient. Other loss generating effects have to be considered and the possibility being able to distinguish between the causes of particular loss components is indispensable. Parasitic loss mechanisms additionally contributing to the total losses originating from field harmonics, non-linear material behaviour, rotational magnetizations, and detrimental effects caused by the manufacturing process or temperature, are not explicitly considered in the common iron-loss models, probably even not specifically contained in commonly used calibration factors. This paper presents a methodology being able to distinguish between different loss mechanisms and enables to individually consider particular loss mechanisms in the model of the electric machine. A sensitivity analysis of the model parameters can be performed to obtain information about which decisive loss origin for which working point has to be manipulated by the electromagnetic design or the control of the machine.

**Key words:** efficiency maps, material degradation, magnetic losses, magnetic material behaviour, soft magnetic materials, electrical machines

## 1. Introduction

The material utilization in electrical machines driven as speed variable drives is dependent on the drive cycle of the machine's application. As a consequence optimizing the drive for a specific working point might not lead to the best machine design for the desired application. For instance, in order to determine the overall efficiency for an entire drive cycle all working points have to be considered including their frequency of occurrence. These findings are certainly not recent and are usually considered by the motor designer.

However, the detailed knowledge of the different loss mechanisms, e.g., the iron losses, can enable the possibility to exploit specific loss effects to enhance the drive in particular working points or for specific operational conditions. On the other hand the most appropriate material choice can be realized with this specific knowledge [1].

In numerical simulations of electrical motors, various material models can be employed to obtain realistic data for the iron losses. In such models, there are basically single components of hysteresis, eddy current and excess losses [2-4] specified. Specific empiric factors calibrate such formula to the particular material operated at defined frequency and polarization. In highly utilized and speed variable drives, this approach is rather inaccurate and therefore inappropriate [5].

To further enhance the properties of electrical motors the accurate determination by idealized model assumptions of the locally distributed iron losses alone is not sufficient [5, 6]. Other iron loss generating effects than hysteresis, Foucault and eddy current losses have to be considered. Further on, it is indispensable to distinguish between the causes of these particular loss components.

Effects which are manufacturing or process dependent can, e.g., roughly be allocated to the cutting, respectively punching process, to imposed mechanical stress to the material or can be temperature dependent.

Following the afore-mentioned reasoning, an improved estimation of iron losses is indispensable, which is applicable in a wide range of frequency and flux density [5]. In addition, parasitic loss inducing effects, particularly occurring in electrical machines, such as higher harmonics, dc-biased magnetizations and rotational fields need to be taken into account [6, 9].

Likewise, the mechanical properties get more and more important: for reasons of yield strength and for processing reasons. The deteriorating effect of material processing, such as guillotine shear, laser (CO2, fibre, Nd:YAG), water abrasive, spark erosion cutting and punching, needs to be included in the iron-loss calculation [7, 8].

Depending on the operating point in electrical machines, copper losses and iron losses have a different share in the overall loss. For high torques, i.e., high electric currents the Ohmic losses are dominant. For high speeds, i.e., high operating frequencies the iron losses dominate. Therefore, the iron losses are one major loss component in inverter driven machines.

The local loss distribution within the machine is important in permanent magnet excited machines. Although the losses dissipated in the rotor make a small contribution of the overall losses, they have to be analysed in particular because of the influence of temperature on the permanent magnets. Depending on the operating point, the rotor hysteresis losses make a significant share in the rotor iron losses [9].

This paper presents a methodology being able to distinguish between different loss mechanisms and enables to individually consider particular loss mechanisms in the model of the electrical motor. With this, a sensitivity analysis of the model parameters can be performed to obtain information about the dominating loss origin in each working point. This enables to manipulate the electromagnetic design of the machine or the control of the motor's electric quantities to enhance the properties, e.g., the efficiency of the machine.

This paper is structured as follows. Section II introduces the main iron-loss modelling approach and its parameter identification procedure. Further on, exemplary modelling results for a non-oriented electrical steel grade are provided.

Section III transfers the iron-loss modelling routine into the machine simulation and shows the machine simulation strategy focused on loss-calculation. Section IV applies the proposed methodology to a permanent magnet synchronous machine simulation. Further on, the local loss distribution and the importance of iron losses is discussed. Finally, Section V includes a discussion of the results and points out the scope for future work.

## 2. Prediction of iron losses

Soft magnetic materials are standardized by international standards [10, 11] using only one value of the specific iron losses for one frequency and one magnetic flux density. Materials with a sheet thickness of 1.0 mm to 0.35 mm are graded by a loss measurement for a frequency of 50 Hz and a magnetic polarization of 1.5 T [10]. Materials with a thicknesses of 0.2 mm to 0.05 mm are characterized at 400 Hz and 1.0 T [11].

For the estimation of iron losses for other values of flux density and frequency than the standard values, several iron-loss models are available. These models can be divided into empirical and physical based approaches.

As a rule of thumb the formulation given in [2] is valid for magnetic flux densities $B \leq 1.2$ T and frequencies $f \leq 400$ Hz [5]. With respect to this, an iron-loss formula (1) has been developed to improve the accuracy at higher frequency and flux density values [5]:

$$P_{IEM,5} = a_1 B^{\alpha} f + a_2 B^2 f^2 \left(1 + a_3 B^{a_4}\right) + a_5 B^{1.5} f^{1.5} \tag{1}$$

with the material specific parameters $\alpha$ and $a_1$ to $a_5$. In addition, the non-linear behaviour of the quasi-static loss contribution [14] as well as the definition of the eddy current loss parameter due to the simplifications [15] was identified as a source of inaccuracy.

Parameter identification is done in line with the physical interpretation of the phenomena. Parameter describing pure hysteresis losses $\alpha$, $a_1$ are identified by quasi-static measurements [17] using an Epstein frame with 1200 turns. The specimen under test is a set of mixed strips (half of them cut along the rolling direction and half cut along transverse direction). According to [17], the change of the magnetic flux density is set to

$$\frac{dB}{dt} = 30 \frac{mT}{s}$$

to ensure quasi-static behaviour. The parameters for pure hysteresis $\alpha$, $a_1$ are identified by a mathematical approximation on the measured quasi-static magnetization energy ($a_1 B^{\alpha}$) and magnetic flux density $B$.

The classical eddy current parameter $a_2$ is calculated by means of (2) using material characteristics $d$, $\rho$, $\rho_e$, which are identified by a standardized process [18].

$$a_2 = \frac{\pi^2 d^2}{6\rho\rho_e}. \tag{2}$$

The excess loss parameter $a_5$ is determined from measurements for frequencies $f \leq 20$ Hz, i.e., at frequencies where the influence of induced Foucault eddy currents is negligible (dependent on the material characteristics) and magnetic flux densities 0.4 T $\leq B \leq$ 1.2 T using the same measurement setup as described for the quasi-static measurements and the procedure described in [19].

The iron loss behaviour in this range of frequency and magnetic flux density is dominated by the hysteresis and excess losses. Since the hysteresis losses are already known, the excess loss term is separated. From the excess losses the parameter $a_5$ is found.

The identification of parameters $a_3$ and $a_4$ describing the losses from non-linear material behaviour is based on the identification of the non-linear loss contribution. Therefore, the losses due to material non-linearity $P_{NL}$ are calculated by the difference of measured losses and sum of calculated hysteresis loss, Foucault eddy current loss, and excess loss. The values of the iron loss parameters of the material studied is given in Table 1.

The IEM-Formula (1) is compared to standard measurements using the parameter set given in Table 1, i.e., measurements with sinusoidal magnetic flux density waveform. The Epstein measurement results in an experimental iron-loss value corresponding with the sinusoidal magnetic flux density waveform. On the other hand, the IEM-Formula (1) is applied to these conditions by the given values for the frequencies and the flux density amplitudes. The modelled loss values are benchmarked against the experimental value (Fig. 1).

Table 1. Loss parameters

| | | |
|---|---|---|
| $\alpha = 1.801$ | $a_2 = 34.648 \cdot 10^{-6}$ | $a_4 = 6.149$ |
| $a_1 = 20.322 \cdot 10^{-3}$ | $a_3 = 30.489 \cdot 10^{-3}$ | $a_5 = 0.34 \cdot 10^{-3}$ |

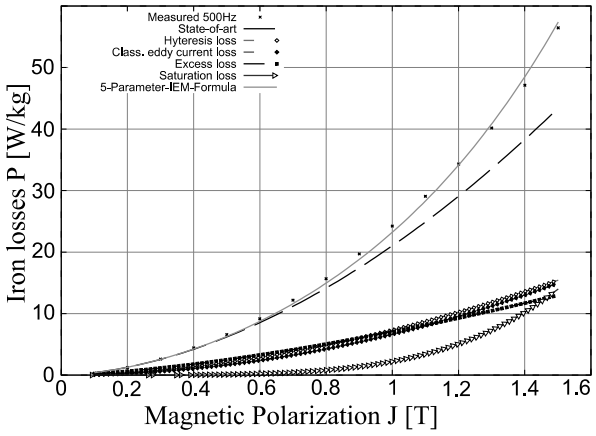


Fig. 1. Iron losses from Epstein measurements and modelled losses

With regard to the operating conditions of electrical machines, other loss generating effects have to be considered. Epstein measurements are performed under uniaxial (spatial) and sinusoidal (temporal) magnetic flux density. Thus, magnetic flux density in Epstein frame measurements is completely represented by its fundamental wave.

However, the design and operation of rotating electrical machines leads to distortions of the fundamental waveform: higher harmonics (in time) due to iron saturation, skin effect, stator yoke slots and the use of a power electronics supply (inverter, PWM) can occur, as well as vector magnetic fields (in space), the latter giving rise to so-called rotational losses.

In order to improve common iron-loss models to these conditions, rotational losses and higher harmonics have to be considered by [6, 21-24]:

1) A Fourier analysis of the magnetic flux density waveform during one electrical period to identify the higher harmonics;
2) The level of magnetic flux distortion and also the (technical) saturation. Two parameters $B_{\min}$ and $B_{\max}$, respectively the minimal and maximal magnetic flux density amplitudes over one electrical period, serve for this.

The locus of the magnetic flux density vector over one electrical period is characterized by $B_{\min}$ and $B_{\max}$. This enables to identify the level of magnetic flux distortion by taking the ratio between $B_{\min}$ and $B_{\max}$. $B_{\max}$ gives an idea about the level of saturation. Zones within the stator with rotational hysteresis are those with large values of $B_{\min}$, whereas unidirectional field corresponds with a zero value of amplitude $B_{\min}$.

Considering this, the hysteresis losses are affected by rotational magnetization, the classical eddy current losses are influenced by higher harmonics in the flux density and excess losses are increased by rotational magnetisation as well as by higher harmonics. To include these effects, the loss contributions of (1) are extended to:

$$P_{Hyst} = a_1 \cdot \sum_{n=1}^{\infty} \left( \left( B_{n,x}^2 + B_{n,y}^2 \right)^{\frac{\alpha}{2}} \cdot nf \right), \tag{3}$$

$$P_{Eddy} = a_2 \cdot \left( \sum_{n=1}^{\infty} \left( B_{n,x}^2 + B_{n,y}^2 \right) \cdot (nf)^2 \right), \tag{4}$$

$$P_{Exc} = a_5 \cdot \left( 1 + \frac{B_{\min}}{B_{\max}} \cdot \left( r_{Exc}\left( B_{\max} \right) - 1 \right) \right) \cdot \left( \sum_{n=1}^{\infty} \left( B_{n,x}^2 + B_{n,y}^2 \right)^{0.75} (nf)^{1.5} \right), \tag{5}$$

$$P_{NL} = a_2 \cdot a_3 \cdot B_{\max}^{2+a_4} \cdot f^2 \tag{6}$$

with $B_{\max}$ the maximum value of the flux density during one period, $B_n$ the amplitude of the $n$-th harmonic component of the magnetic flux density, $n$ the order of harmonic, $f$ the fundamental frequency, and the material specific parameters $\alpha$, $a_1 - a_5$. This model (3-6) is validated in [9, 20] and will be used to analyse the iron losses in the studied IPMSM.

## 3. Machine simulation scheme

In order to understand the influence of machine design of a traction drive it is not sufficient to consider one operating point. Therefore, the entire operating range of the machine is simulated.

The operating behaviour is determined by the interaction of the stator- and the rotor flux linkage. In case of a permanent magnet synchronous machine, the length and direction of the rotor excitation flux vector is defined by the permanent magnets.

In order to depict the complete operation space the stator flux vector, respectively the stator current vector must be varied during simulation. For this purpose the rotor-flux-fixed dq-reference frame is used to perform a variation of the direct and the quadrature current.

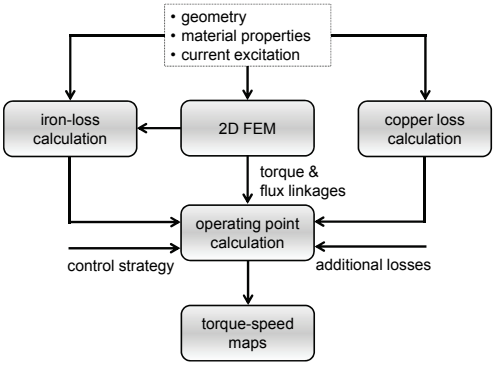


Fig. 2. Machine simulation scheme

Figure 2 gives an overview of the machine simulation scheme. Starting from the geometry of the studied machine in combination with its material properties (remnant induction of permanent magnets, magnetization behaviour of soft magnetic material, iron-loss parameters), the direct and quadrature currents are varied. For each combination of direct and quadrature current the corresponding electro-magnetic torque, magnetic flux-linkage and local magnetic flux density distribution is calculated.

Based on the local magnetic flux density distribution the iron-losses are calculated according to (9-12). Finally, combining the modeled iron losses with additional losses (copper, air friction, bearing, …), the operation point of the machine is calculated in line with the used control strategy, i.e., maximum-torque-per-ampere (MTPA) or maximum-torque-per-voltage (MTPV). Boundaries resulting from voltage or current limit are taken into account.

Using this detailed information, the iron-loss distribution is calculated and analysed in each working point across the torque-speed map of the machine. In the following section this scheme is exemplarily applied to an interior permanent-magnet synchronous machine designed for an automotive traction application.

## 4. Permanent-magnet synchronous machine

The IEM-Formula (9-12) in combination with the simulation scheme (Section III) is exemplarily employed to a permanent magnetic synchronous machine for automotive application (Fig. 3).

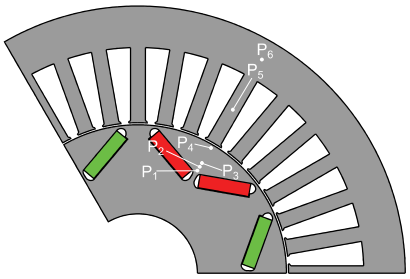


Fig. 3. Cross section of the studied machine

The studied machine with V-shaped permanent-magnets inside the rotor has a maximum rotational speed of $n_{max}$ = 18000 rpm, a maximum torque of $M_{max}$ =140 Nm, a maximum current of $I_{max}$ = 300 A, and operates at a dc-link voltage of $U_{dc}$ = 400 V.

In particular, in highly utilized electrical machines operating as traction drives, iron losses are important, as will be detailed in this section. Depending on torque, rotational speed and frequency the dominating loss terms change.

Single-valued magnetization curves have been used in the 2D FEM simulation to consider saturation effects originating from the non-linear material behaviour. Second-order effects, originating from hysteresis behaviour, are neglected. Pure hysteresis, classical eddy current, excess as well as saturation losses (9-12) in the laminated stator and rotor cores are estimated a posteriori.

In order to apply the described iron-loss model the spatial vector field and the parasitic effects through higher harmonics need to be taken into account. For this purpose the local waveforms of the magnetic flux densities at different positions in the electrical machine are analyzed.

Figures 4 to 6 present the magnetic flux density in different loci of the machine cross-section (Fig. 3) exemplarily at 100 Nm in the base speed range of 6000 min$^{-1}$. $P_1$ to $P_4$ are located inside the rotor of the machine. It is apparent that the magnetic flux density behaviour is shifted with a dc-bias offset due to the remanent magnetic flux density of the permanent magnets and the magnetic field from direct axis current. Point $P_1$ is directly related to the by-pass-flux of the permanent magnets.

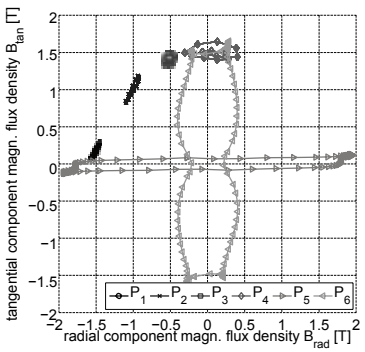


Fig. 4. Locus of magnetic flux density during one period in different points of interest

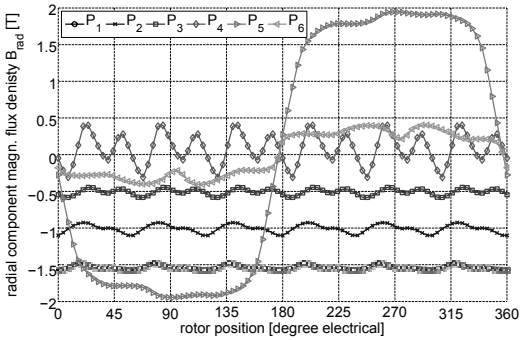


Fig. 5. Radial component of magnetic flux density during one period in different points of interest in the cross-section of the studied machine

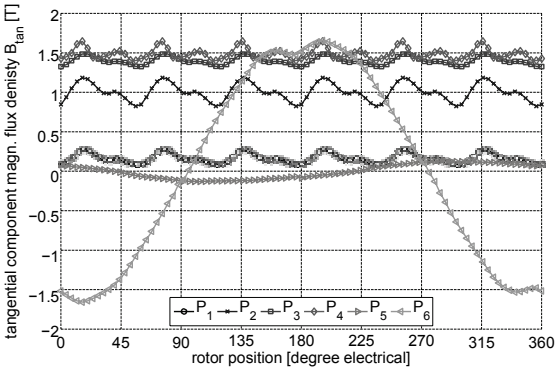


Fig. 6. Tangential component of magnetic flux density during one period in different points of interest in the cross-section of the studied machine

Point $P_4$ represents the tangential pre-magnetization due to quadrature current, whereas points $P_2$ und $P_3$ depict a mixture of the afore-mentioned components. In combination with Figures 5 and 6 it is apparent, that at points $P_1$ to $P_4$ no complete magnetization cycle is passed through during one electrical period, i.e., the resulting magnetization cycle is a minor loop.

In [9] it is shown that neglecting of minor-loop hysteresis losses inside a permanent magnet synchronous machine leads to an underestimation of rotor iron losses of about 50%. On that account, it should be stressed that an accurate iron-loss calculation in a permanent-magnet synchronous machine rotor needs to include minor-loop hysteresis [9].

Points $P_5$ and $P_6$ are located in the stator. At $P_5$ located in the centre of a stator tooth the magnetic flux density is almost entirely directed along the radial direction. The tangential component is significantly smaller, i.e., $B_{\mathrm{rad}}$ reaches a maximum of 1.95 T, whereas the tangential component $B_{\mathrm{tan}}$ reaches less than 0.13 T.

It is apparent that in the base of a tooth ($P_6$), i.e., in the region where the magnetic flux heads from the yoke to the tooth or vice versa, to some extent rotational magnetization processes occur with $B_{\mathrm{tan}}$ of 1.65 T and $B_{\mathrm{rad}}$ of 0.4 T. Furthermore the non-sinusoidal time-behaviour is clearly recognizable.

Next to this, the influence of the machine operation is discussed in detail. The machine is modelled in a rotor-flux fixed dq-reference frame. In order to calculate the operating points of the machine the maximum torque per ampere (MTPA) control strategy for the base speed range ($n < 6{,}000$ min$^{-1}$). For the field weakening range ($n > 6000$ min$^{-1}$) the MTPA formulation with an additional speed depending upper boundary for the stator flux linkage is used [20, 25].

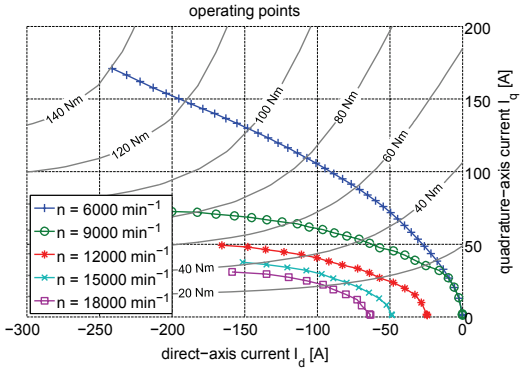


Fig. 7. Operating points of the studied machine

In Figure 7 the operational characteristics of the studied machine, including the operating points at different rotational speeds, are given. When going to higher rotational speeds an increased field-weakening is necessary, i.e., increased negative direct current and decreased quadrature current to reach the same torque.

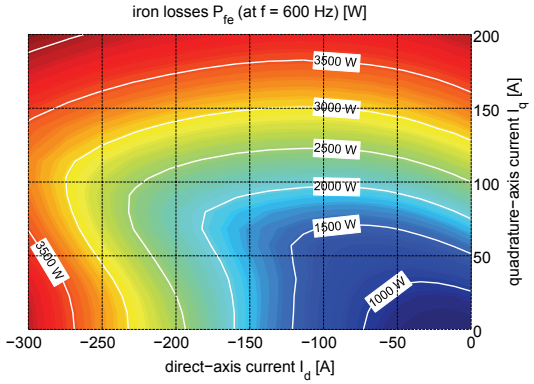


Fig. 8. Iron losses at a fixed fundamental frequency of 600 Hz (12000 min$^{-1}$)

Figure 8 depicts the iron losses at a fixed rotating speed of 12000 min$^{-1}$, i.e., in field weakening operation. An increase in current and thus also an increase in flux density results in an increase of iron losses. It is shown that the influence of quadrature current and direct current on the iron losses is different. Figure 8 shows the influence of direct and quadrature axis current on iron losses is highly depending on the working point of the machine.

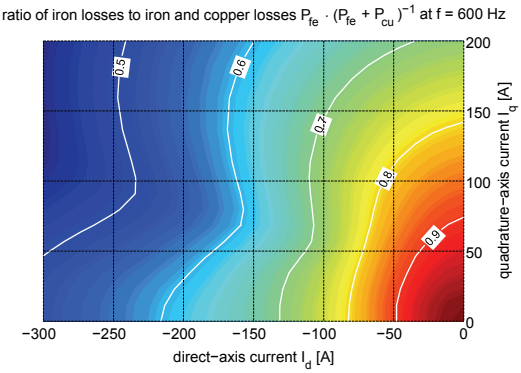


Fig. 9. Ratio of iron losses and the sum of iron and copper losses at a fixed frequency of 600 Hz (12000 $min^{-1}$)

Since the increased currents lead to an increase in copper losses, it is necessary to check the distribution between iron and copper losses and their percentage distribution. Figure 9 underlines that the iron losses increase less strongly with the current than the copper losses, which are proportional to the current squared. Hence, in order to characterize the operating behaviour of an electrical machine it is important to include MTPA and field weakening operation in the determination of a torque-speed map.

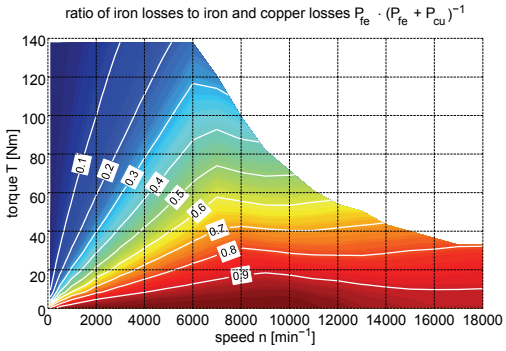


Fig. 10. Ratio of iron losses and the sum of iron and copper losses across the entire torque-speed range of the studied machine

The importance of a detailed examination of the iron losses is emphasized by Figure 10. Initially the proportion of the iron losses rises significantly in the base speed range. Reaching the field-weakening range the rise is despite increasing rotational speed less significant due to higher stator currents and reduced stator flux linkage values and therefore lower flux density values.

Figure 11 depicts the total loss distribution across the whole torque-speed map of the studied electrical machine. In addition characteristic working areas are indicated by ellipses. In the area of high torque and low frequencies a high acceleration is achieved. The operating area

of the machine for a city drive is located at low frequencies and medium torque, while the area for a highway drive is located at high frequencies and low to medium torque.

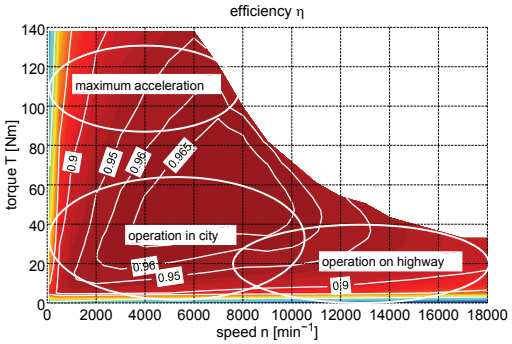


Fig. 11. Torque-speed efficiency map of the studied machine. Ellipses indicate operation modes

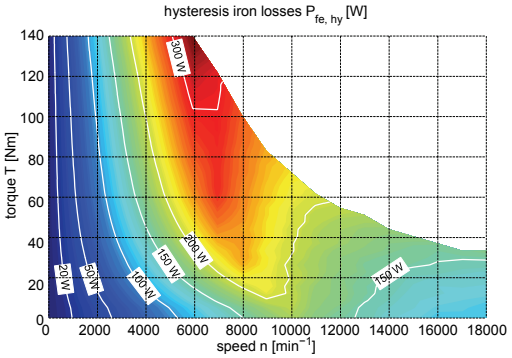


Fig. 12. Hysteresis loss distribution across the torque-speed map

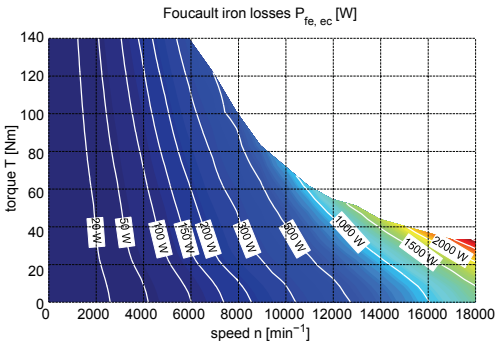


Fig. 13. Foucault eddy current loss distribution across the torque-speed map

When selecting the soft magnetic materials, the frequency distribution of operating points of the application can be taken into account. Figures 12 to 15 illustrate the separate loss terms

of the iron losses (9-12). While the hysteresis losses (Fig. 12) and nonlinear losses (Fig. 15) dominate the middle frequency and high torque range, the classical eddy current losses (Fig. 13) as well as the excess losses (Fig. 14) have in the range of high frequencies their biggest impact.

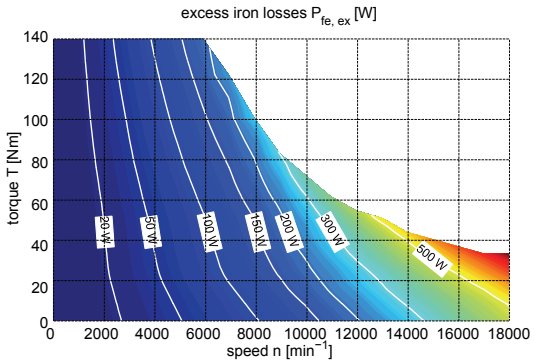


Fig. 14. Excess eddy current loss distribution across the torque-speed map

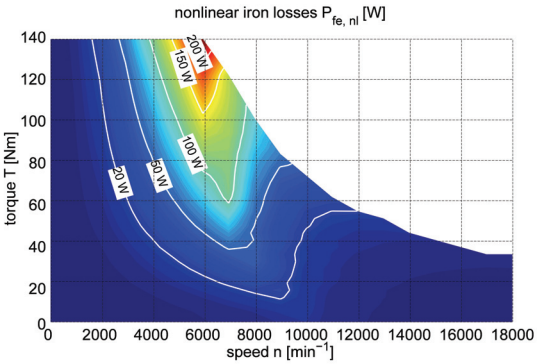


Fig. 15. Saturation eddy current loss distribution across the torque-speed map

The afore-mentioned analysis underlines the importance of a differentiated consideration of the iron-loss distribution across the whole torque-speed map, when aiming at an improvement of the electrical machines' properties. A consideration of the locally distributed iron losses alone is not sufficient. It is indispensable being able to distinguish between the causes of particular loss components.

## 5. Conclusions

This work presents a general approach for rigorous understanding of material characteristics in electrical machines. In particular, the iron losses have to be analysed regarding their

loss mechanism and their local distribution. This enables to increase power density and custom-designed drive characteristics. Further on, the local loss distribution allows for development of tailor-made soft-magnetic materials. The approach being able to distinguish between different loss mechanisms enables to individually consider particular loss mechanisms in the model of the electric motor particular.

With this, a sensitivity analysis of the model parameter can be performed to identify dominating loss mechanisms with the objective of design adjustments in any stage of the production process of electrical machines. The flexibility of the iron-loss model allows for consideration of parasitic loss mechanisms additionally contributing to the total losses, such as the manufacturing process [26-30]. Since at prototyping stage of electrical machines mostly other manufacturing processes are used than in mass series production, the influence from manufacturing can be taken into account and a prediction of the behaviour of a series produced machine can be derived.

## References

[1] Podoleanu I., Schneider J., Müller G., Hameyer K., *Software tool for the optimum material choice for induction machines.* Proc. Conf. OPTIM (2002).
[2] Bertotti G., *Hysteresis in magnetism*. Academic Press (1998).
[3] Steinmetz C., *On the law of hysteresis* (originally published in 1892). Proc. Conf. IEEE 72(2): 197-221 (1984).
[4] Zirka S.E., Moroz Y.I., Marketos P., Moses A.J., *Loss Separation in Nonoriented Electrical Steels.* IEEE Trans. Magn. 46(2) (2010).
[5] Jacobs S., Hectors D., Henrotte F. et al., *Magnetic material optimization for hybrid vehicle PMSM drives*. Proc. Conf. EVS24 (2009).
[6] Steentjes S., Leßmann M., Hameyer K., *Advanced Iron-Loss Calculation as a Basis for Efficiency Improvement of Electrical Machines in Automotive Application.* Proc. Conf. ESARS, pp. 1-6 (2012).
[7] Henrotte F., Schneider J., Hameyer K., *Influence of the manufacturing process in the magnetic properties of iron cores in induction machines*. Proc. Conf. WMM (2006).
[8] Steentjes S., Hameyer K., Bednarz M. et al., *Influence of material processing steps annealing and cutting on magnetic materials' properties relevant for electrical machine design*. Proc. Conf. FTF (2013).
[9] Steentjes S., von Pfingsten G., Hombitzer M., Hameyer K., *Iron-loss model with consideration of minor loops applied to FE-simulations of electrical machines*. IEEE Trans. on Magn. 49(7) (2013).
[10] Standard DIN EN 10106: *Cold rolled non-oriented electrical steel sheet and strip delivered in the fully processed state*. Beuth Verlag (2007).
[11] Standard DIN EN 10303: *Thin magnetic steel sheet and strip for use at medium frequencies.* Beuth Verlag (2001).
[12] Steinmetz C., *On the law of hysteresis* (originally published in 1892). Proc. IEEE 72(2): 197-221 (1984).
[13] Bertotti G., *General Properties of Power Losses in Soft Ferromagnetic Materials*. IEEE Trans. on Magn. 24(1): 621-630 (1988).
[14] Moses A.J., *Energy efficient electrical steels: Magnetic performance prediction and optimization*. Scripta Materialia 67: 560-565 (2012).
[15] Landgraf F.J.G., de Campos M.F., Leicht J., *Hysteresis loss subdivision.* Journal of Magnetism and Magnetic Materials 320: 2494-2498 (2008).
[16] Gyselinck J., Vandewelde L., Melkebeek J. et al., *Calculation of Eddy Currents and Associated Losses in Electrical Steel Laminations*. IEEE Trans. on Magn. 35(3): 1191-1194 (1999).

[17] De Wulf M., Dupré L., Melkebeek J., *Quasistatic measurements for hysteresis modeling*. Journ. Appl. Phy. 87(9): 5239-5241 (2000).
[18] Standard DIN IEC 60404-13: *Magnetic materials – Part 13: Methods of measurement of resistivity, density and stacking factor of electrical steel strip and sheet.* Beuth Verlag (2015).
[19] Standard DIN IEC 60404-2: *Magnetic materials – Part 2: Methods of measurement of the magnetic properties of electrical steel strip and sheet by means of an Epstein frame*. Beuth Verlag (2009).
[20] G. von Pfingsten, T. Herold, K. Hameyer, *Kalibrierte Leistungssimulation von elektrischen Maschinen – eine Möglichkeit zur Bewertung von nicht vermessbaren Betriebsbereichen und des Einsatzes unterschiedlicher weichmagnetischer Materialien ohne weiteren Musterbau*. Proc. Nat. Conf. VDE/VDI Antriebssysteme (2013).
[21] Bertotti G., Canove A., Chiampi M. et al., *Core loss prediction combining physical models with numerical field analysis.* Journ. .Magn. and Magn. Mat. 133: 647-650 (1994).
[22] Fiorillo F., Novikov A., *An Improved Approach to Power Losses in Magnetic Laminations under Nonsinusoidal Induction*. IEEE Trans. on Magn. 26(5): 1990.
[23] Fiorillo F., Novikov A., *Power losses under sinusoidal, trapezoidal and distorted induction waveform*. IEEE Trans. on Magn. 26(5): 2559-2561 (1990).
[24] Fiorillo F., Rietto A.M., *Rotational versus alternating hysteresis losses in nonoriented soft magnetic laminations.* Journ. Appl. Phy. 73: 6615-6617 (1993).
[25] De Doncker R., Pulle D., Veltman A., *Advanced Electrical Drives: Analysis.* Modelling, Control, Springer (2010).
[26] Baudouin P., Belhadj A., Breaban F. et al., *Effects of laser and mechanical cutting modes on the magnetic properties of low and medium Si content non-oriented electrical steels*. IEEE Trans. on Magn. 38(5): 3213-3215 (2002).
[27] Schmidt K.-H., *Influence of punching on the magnetic properties of electric steel with 1% silicon*. Journ. Magn. Magn. Mat. 2: 136-150 (1976).
[28] Schoppa A., Schneider J., Wuppermann C.D., *Influence of the manufacturing process on the magnetic properties of non-oriented electrical steels*. Journ. Magn. Magn. Mat. 215-216: 74-78 (2000).
[29] Moses A.J., Derebasi N., Loisos G., Schoppa A., *Aspects of the cut-edge effect stress on the power loss and flux density distribution in electrical steel sheets*. Journ. Magn. Magn. Mat. 215-216: 690-692 (2000).
[30] Vandenbossche L., Jacobs S., Henrotte F., Hameyer K., *Impact of cut edges on magnetization curves and iron losses in e-machines for automotive traction*. EVS-25 (2010).